RSC Advances

PAPER

View Article Online
View Journal | View Issue

Cite this: *RSC Adv.*, 2021, **11**, 20992

Viscosity effect on the strategic kinetic overgrowth of molecular crystals in various morphologies: concave and octapod fullerene crystals†

Kwangjin Song, Jin Young Koo and Hee Cheul Choi *

A kinetic overgrowth allowing organic molecular crystals in various morphologies is induced by temperature-dependent viscosity change of crystallization solution. By this strategy, concave cube and octapod fullerene C_{70} crystals were successfully obtained by antisolvent crystallization (ASC). The structural analysis of fullerene C_{70} crystals indicates that the morphological difference is the result of kinetic processes, which reveals that viscosity, the only variable that can change dynamics of solutes, has a significant influence on determining the morphology of crystals. The effect of solvent viscosity in the stage of crystal growth was investigated through time-dependent control experiments, which led to the proposal of a diffusion rate-based mechanism. Our findings suggest morphology control of organic crystals by diffusion rate control, which is scarcely known compared to inorganic crystals. This strategic method will promote the morphology controls of various organic molecular crystals, and boost the morphology–property relationship study.

Received 15th April 2021
Accepted 4th June 2021

DOI: 10.1039/d1ra02924j

rsc.li/rsc-advances

Because morphology directly affects the properties of crystals, morphology control of crystals has been one of the major research subjects in chemistry. While the strategies for the morphology control of inorganic metal crystals have been established quite well in the solution phase, primarily through surface chemistry guiding crystallization to occur only on non-passivated crystal planes or through kinetic overgrowth,[1–3] the absence of such strategic methods controlling the morphology of organic molecular crystals restricts their potential. Thus, enormous efforts have been devoted to exploring new approaches to control the morphology of molecular crystals through solvent[4,5] and temperature controls.[6,7]

As frequently demonstrated from inorganic metal crystals, kinetic overgrowth can be a prominent method to obtain molecular crystals in various shapes. The kinetic overgrowth induces preferred growth at specific sites resulting in morphologies that are not available thermodynamically, as demonstrated from concave cubes and octapods.[8–13] The kinetic overgrowth usually occurs with a concentration gradient around the seed crystals, which can be achieved by regulating the diffusion rate (V_{diff}) of solutes and crystal growth rate (V_{grow}). Therefore, it is important to understand and develop kinetic overgrowth process for organic molecular crystals, which can correspond to the well-established surface chemistry for inorganic metal crystals.

Considering the importance of concentration gradient near seed crystals for kinetic overgrowth, among various crystallization methods, antisolvent crystallization (ASC) process in which supersaturation and nucleation are induced by the injection of antisolvent to which target molecules have a low solubility (Scheme 1),[14–18] is an ideal method for kinetic overgrowth of molecular crystals since it has many variables that can change micro-environment near seed crystals. In addition, fullerenes are good target molecules because obvious results are expected when kinetic product is successfully contrasted to well-known thermodynamic morphologies such as tubes, rods, and even polyhedrons,[19–23] as Yang *et al.* and Ariga *et al.* showed.[24–26] In this case, kinetically favorable fullerene concave cubes could be formed by involving sonication[24] and controlling solvent

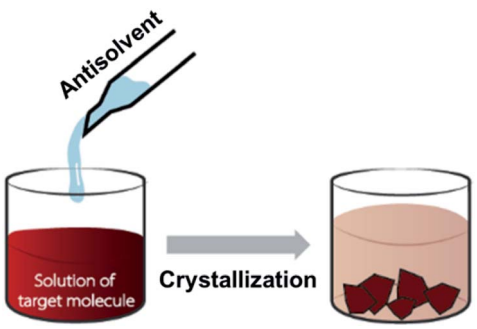

Scheme 1 Schematic illustration of traditional ASC process. Target molecules are effectively crystallized *via* solvation shell mechanism.

Department of Chemistry, Pohang University of Science and Technology (POSTECH), Pohang 37673, Republic of Korea. E-mail: choihc@postech.edu

† Electronic supplementary information (ESI) available. See DOI: 10.1039/d1ra02924j

ratio,[25,26] and clearly contrasted with fullerene cube crystals. However, the origin and detailed mechanism of these kinetic overgrowths are still veiled, which prevents further application.

In this regard, the influence of temperature on kinetic overgrowth of organic molecular crystals should be investigated not only because of its contribution for thermodynamic *versus* kinetic reaction control in many branches of chemistry,[27–29] but also because it can alter the behavior of molecules significantly during ASC, especially by regulating solution viscosity. Therefore, in this study, we aim to investigate the effect of viscosity upon temperature change for kinetic overgrowth of fullerene crystals. Herein, we show that kinetic overgrowth can be induced by controlling temperature in ASC. Kinetically overgrown fullerene C_{70} crystals, in concave cube and octapod shapes, are successfully obtained at low temperature, while only cube crystals are obtained at higher temperature. These results originate from increased solution viscosity, which causes slow diffusion of C_{70} molecules to seed crystals, and consequent kinetic overgrowth. Diffusion rate-based mechanism of inorganic metal nanocrystals is successfully applied to this strategic morphology control.

All the fullerene crystallization has been performed by ASC method. Isopropanol (IPA), an antisolvent, is added to C_{70} solution in mesitylene to obtain cube-shaped C_{70} crystals at room temperature. After 3 h, black precipitates have been separated from the solution by filtration for characterization. Well-defined faces, edges, and vertices of C_{70} cubes are confirmed using a scanning electron microscope (SEM), which agrees well with previous report (Fig. 1a).[19] To investigate the effect of growth temperature on the morphology, ASC of C_{70} has been performed at lower temperature. When the growth temperature is lowered from RT to −16 °C using a refrigerator and −78 °C using dry ice bath, concave cube-shaped and unprecedented octapod C_{70} crystals are obtained, respectively (Fig. 1b and c). The average sizes of the C_{70} cube, concave cube, and octapod are 2.0 μm, 2.5 μm, and 1.7 μm, respectively (Fig. S1†). The resulting crystals show a high degree of homogeneity in their morhpologies.

Because these morphologies are well-known kinetically overgrown products for inorganic metal nanocrystals,[8–13] we have checked the viscosity of crystallization solution at each temperature, which is directly related to V_{diff} of C_{70} molecules by the Stokes–Einstein equation.[30] The apparent viscosity of the solution at the shear rate of 1000 Hz increases from 2.05 cp to 6.40 cp at −16 °C and further to 218.36 cp at −78 °C (Fig. 1d), which indicates dramatic decrease of V_{diff} of C_{70} molecules may occur. From these results, it can be assumed that this morphology difference comes from the slow diffusion of C_{70} molecules, which is induced by high viscosity at low temperature.

The crystal structures of each product have been examined by powder X-ray diffraction (Fig. 2a). For C_{70} cube crystals, the overall diffraction pattern including the intense peak from (100) plane with *d*-spacing of 10.56 Å indicates a simple cubic structure as known from previous results.[19] Importantly, the XRD patterns of C_{70} concave cube and octapod crystals are the same as cube crystals, which implies that the concave cube and octapod morphologies are the results of kinetic crystal overgrowth from cube crystals.[25]

Furthermore, to examine the effect of solvent inclusion on the crystal morphologies,[22] the intercalated molecules have

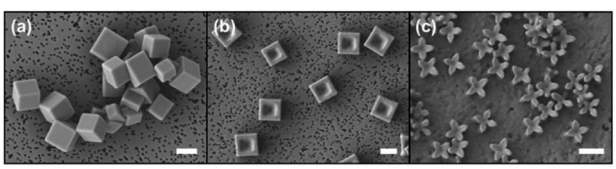

(d)

Temperature	25 °C	-16 °C	-78 °C
Viscosity	2.05 cp	6.40 cp	218.36 cp
Product	Cube	Concave cube	Octapod

Fig. 1 C_{70} crystals prepared by ASC at different conditions. (a) Cubes at 25 °C, (b) concave cubes at −16 °C, and (c) octapods at −78 °C. (d) Crystallization condition and obtained morphology of product (scale bar: 2 μm).

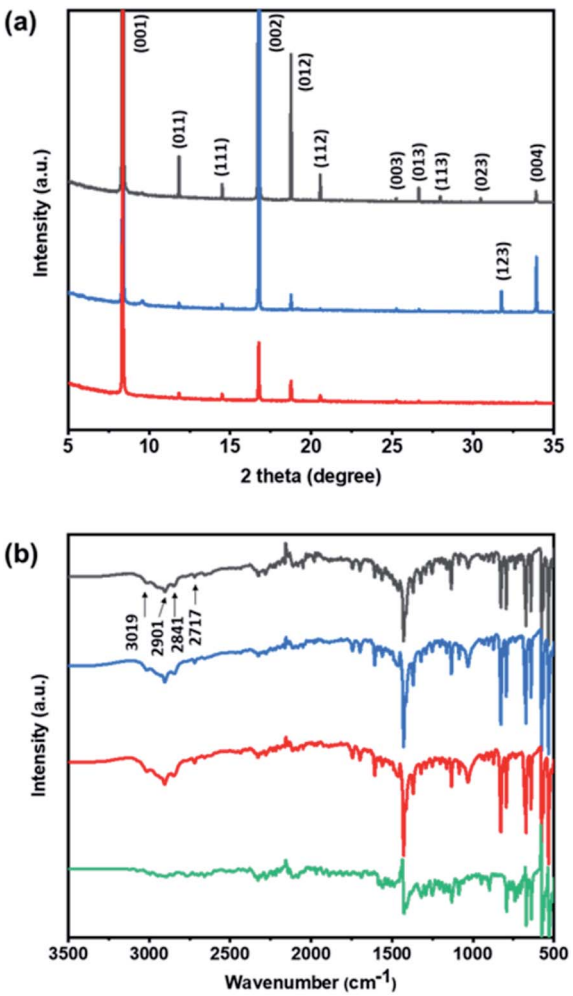

Fig. 2 (a) X-ray diffraction patterns and (b) Fourier transform infrared spectra of C_{70} cubes (black), concave cubes (blue), octapods (red), and pristine powder (green).

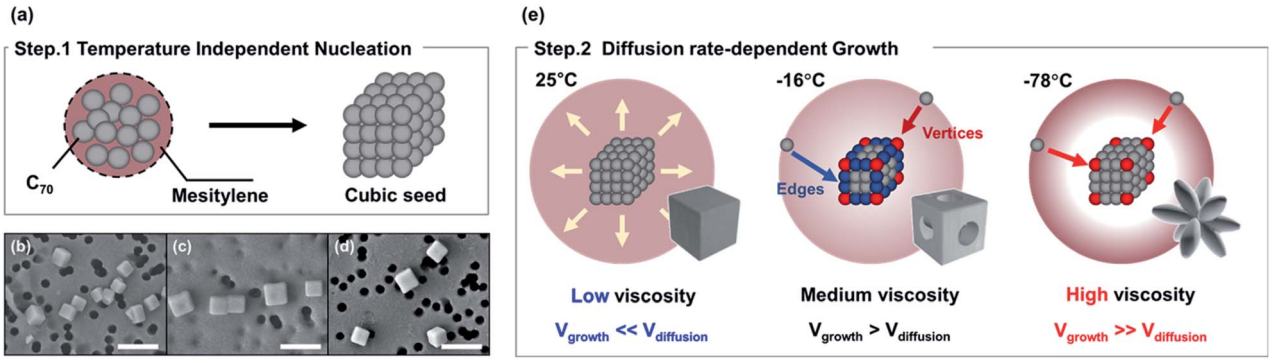

Fig. 3 (a) Schematic illustration of temperature-independent nucleation of C_{70} immediately after the injection of antisolvent, and the SEM images of seed crystals prepared at (b) 25 °C, (c) −16 °C, and (d) −78 °C (scale bar: 500 nm). (e) Schematic illustration of diffusion rate-dependent growth from cubic seed crystals.

been analyzed using Fourier-transform infrared spectroscopy (Fig. 2b). Four representative peaks of mesitylene (2717, 2841, 2901, 3019 cm^{-1}) are observed equally from all three types of C_{70} crystals.[25] This result suggests that the intercalation of solvent is irrelevant to the morphology decision. The influence of intercalated mesitylene on the rotational motion of fullerene is also investigated by Raman spectroscopy, and no peak shift also indicates that the intercalated mesitylene does not affect the motion of fullerene molecules in crystal lattice (Fig. S2†).[25] Therefore, we conclude that morphological diversity of C_{70} crystals is not originated from common structural difference, but from the crystal overgrowth induced by diffusion rate change induced by viscosity change.

The overall mechanism of morphology control during ASC *via* viscosity control can be proposed as follows (Fig. 3). When antisolvent is injected into C_{70} solution of mesitylene, emulsion droplets containing C_{70} and mesitylene are formed instantaneously, followed by the diffusion of mesitylene out to continuous phase consisted of antisolvent (Fig. 3a).[31] As a result, supersaturation and nucleation occur, and seed crystals are formed. To examine if the morphology decision is made at the nucleation stage or growth stage, the seed crystals obtained at 25 °C, −16 °C, and −78 °C are identified by SEM to confirm their cube-shaped morphology (Fig. 3b–d and Fig. S3†). Therefore, the morphological difference must be induced at the crystal growth step, rather than the nucleation step, which is also on the line of seed-mediated kinetic overgrowth mechanism.

After nucleation, the reaction system goes through metastable states, where crystals continue to grow and kinetic overgrowth starts to play. All the mesitylene emulsion droplets are broken and release C_{70} nucleates. Then, C_{70} molecules remained in the continuous phase at the stage of nucleation are attached to the nucleates. In this stage, the competition between V_{diff} of C_{70} molecules and V_{grow} plays a key role in the determination of crystal morphology, where V_{diff} is controlled effectively by viscosity (Fig. 3e). At 25 °C, the viscosity of solution is quite small, so C_{70} molecules can easily diffuse from the bulk solution to the seed crystals ($V_{diff} >> V_{grow}$). In this condition, the concentration of C_{70} around seed crystals is maintained almost same, hence no preferential overgrowth occurs, resulting in seed crystal morphology-retained cube crystals.[19] Whereas, C_{70} molecules cannot diffuse rapidly at −78 °C due to the high viscosity of the solution ($V_{diff} << V_{grow}$). In this regime, the concentration gradient of solute around seed crystals is generated because of the fast consumption of C_{70} molecules near seed crystals with slow refill from the bulk solution. Such a concentration gradient induces preferential attachment of distant solutes to the sites possessing the highest reactivity, vertices for cubic crystals, as known for the inorganic metal crystals.[8–13] Eventually, octapod-shaped C_{70} crystals are formed. The kinetic overgrowth that frequently results in anisotropic crystal growth at specific sites[32–34] rather than thermodynamic isotropic growth resulting in simply bigger crystals was supported from time-dependent SEM images of C_{70} crystals at −78 °C (Fig. 4) showing petals that are preferentially and continuously grown out of cube crystals. In contrast, an isotropic growth only with a size increase from cubic seed has been observed in the case of the growth at 25 °C (Fig. S4 and S5†), which indicates thermodynamic crystal growth at low viscosity.

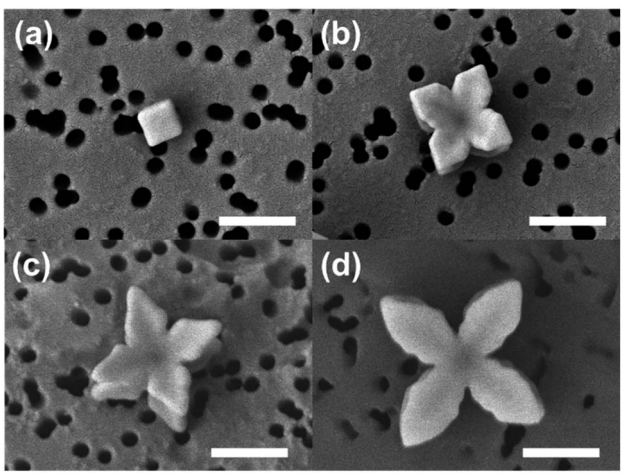

Fig. 4 Time-dependent SEM images of C_{70} octapod crystals obtained at −78 °C. Growth time for each image is (a) 0 min, (b) 1 min, (c) 5 min, and (d) 30 min, respectively (scale bar: 1 μm).

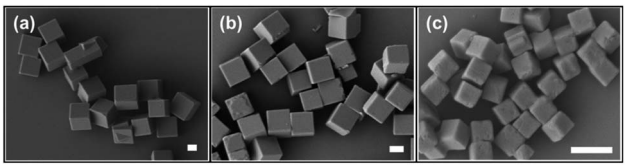

Fig. 5 C_{70} cubes prepared using acetone as antisolvent at (a) 25 °C, (b) −16 °C, and (c) −78 °C (scale bar: 2 μm).

To verify if this morphology control is directly related with viscosity change rather than temperature change itself, control experiments using less viscous solvent at the same temperature have been conducted, finding no morphology changes. When acetone is used as antisolvent instead of IPA, no morphological change is observed even at the growth temperature of −78 °C, (Fig. 5 and S6†) and this result owes to the low viscosity of acetone even at low temperature.[35] In other words, the addition of acetone to mesitylene solution does not cause a dramatic viscosity change, which implies the importance of the selection of good solvent and antisolvent for the successful morphology control by ASC process. On the other hand, the use of other alcohols (ethanol, 1-propanol, and 1-butanol having viscosity of 5.26, 6.52, and 7.53 cp at −16 °C and 30.0, 79.8, and 132.0 cp at −78 °C, respectively) show clear kinetic overgrowth at low temperature (Fig. S7†). Other than the viscosity change inducing morphology control, there is another important property change, *i.e.* solubility change upon temperature change (Fig. S8†) to be considered, which requires further studies in the future.

Conclusions

We reveal that kinetic overgrowth is an effective route to obtain fullerene crystals in various morphologies, concave cube and octapod through kinetic overgrowth. The kinetic overgrowth can be induced by viscosity change of crystallization solution, which is readily available by temperature change. Finding other ways to modulate viscosity of crystallization than temperature change would be the key for the popular usage of kinetic overgrowth method. We are also currently working on the application of kinetic overgrowth to other organic molecules to check its versatility. This work provides new insights into the role of temperature for the morphology control of fullerene crystals by ASC, allowing kinetic overgrowth as a facile way to obtain molecular crystals in various shapes.

Experimental section

Materials

Fullerene C_{70} (MTR LTD, 98+%), mesitylene (Alfa Aesar, 98+%), isopropanol (Sigam Aldrich, anhydrous, 99.5%), ethanol (Samchun, anhydrous, 99.9%), 1-propanol (Sigma Aldrich, for HPLC, ≥99%), 1-butanol (Sigma Aldrich, 99.8%, HPLC grade), and acetone (Sigma Aldrich, for HPLC, ≥99.9%) were purchased and used without further purification.

Preparation of cube-, concave cube-, and octapod-shaped C_{70} crystals using IPA

10 mg of C_{70} powder was dissolved in 10 mL of mesitylene, followed by sonication for 30 min. Pure C_{70} solution without any impurities and undissolved C_{70} powder was obtained by filtration, and 3 mL of this solution was diluted by adding 7 mL of mesitylene. Cube-shaped fullerene C_{70} crystals were synthesized by adding 4 mL of IPA to 1 mL of diluted C_{70} solution. The mixture was shaken by hand for 5 s and kept at 25 °C for designated times. Concave cube- and octapod-shaped fullerene C_{70} crystals were obtained at lower temperature of −16 °C and −78 °C, while other conditions are identical. C_{70}/mesitylene solution was cooled to −16 °C and IPA cooled to −16 °C and −78 °C was added into the C_{70}/mesitylene solution for concave cube and octapod, then mixed vigorously by handshaking and placed in refrigerator and dry ice/acetone bath to keep the reaction temperature at −16 °C and −78 °C, respectively. Note that the crystallization solution at −78 °C is stable despite the high melting point (−45 °C) of mesitylene owing to the melting point depression upon the addition of antisolvent. All resulting crystals were collected *via* filtration.

Testing acetone as antisolvent

1 mL of acetone was injected to 1 mL of diluted C_{70} solution in mesitylene, followed by hand-shaking for 5 s at various temperature (25 °C, −16 °C, −78 °C). The mixtures were kept at each temperature for 3 h, and resulting cubic crystals were collected by filtration.

Testing other alcohols as antisolvent

4 mL of ethanol, 1-propanol, and 1-butanol were injected to 1 mL C_{70} solution in mesitylene with different concentration, followed by hand-shaking for 5 s at various temperature (25 °C, −16 °C, −78 °C). The concentration of C_{70} solution is 0.2, 0.3, and 0.6 mg mL^{-1} when using ethanol, 1-propanol and 1-butanol, respectively. The mixtures were kept at each temperature, and resulting crystals were collected *via* filtration.

Characterizations

Scanning electron microscope (SEM) images were obtained using a JEOL JSM-7401F. Viscosity measurements were performed using a DHR-3 rheometer, with the shear rate of 1000 Hz. Used upper geometry and lower geometry were 25 mm aluminum flat plate and 25 mm stainless steel, stepped lower ETC plate, respectively. Note that the measurement of zero shear viscosity, which describes a plateau viscosity value of material was impossible because of the escape of solution from sample holder at low shear rate. Structural analysis of C_{70} cubes, concave cubes, and octapods was achieved by attenuated total reflectance infrared (ATR-IR) spectroscopy (Thermo Scientific, Nicolet iS50) using diamond crystals, and Raman spectroscopy (WITECH Alpha 300R). X-ray diffraction (XRD) patterns were obtained at the 5D beamline of Pohang Accelerator Laboratory (PAL, Pohang, Korea).

Conflicts of interest

There are no conflicts to declare.

Acknowledgements

This work was supported by Veteran Researcher Grant (no. 2019R1A2C2004259) and Basic Science Research Program (no. 2021R1C1C2006705) through the National Research Foundation of Korea (NRF) and Samsung Electronics. PXRD measurements were performed at the 5D beamline of PAL, and SEM images were obtained at National Institute for Nanomaterials Technology (NINT). Viscosity measurements were fulfilled at Korea Institute of Science and Technology (KIST) Jeonbuk Institute of Advanced Composite Materials.

References

1 D. F. Zhang, H. Zhang, L. Guo, K. Zheng, X. D. Han and Z. Zhang, *J. Mater. Chem.*, 2009, **19**, 5220–5225.
2 J. Pan, G. Liu, G. Q. M. Lu and H.-M. Cheng, *Angew. Chem., Int. Ed.*, 2011, **50**, 2133–2137.
3 J. Lin, W. Hao, Y. Shang, X. Wang, D. Qiu, G. Ma, C. Chen, S. Li and L. Guo, *Small*, 2018, **74**, 1703274.
4 X. Zhang, C. Dong, J. Zapien, S. Ismathullakhan, Z. Kang, J. Jie, X. Zhang, J. Chang, C.-S. Lee and S.-T. Lee, *Angew. Chem., Int. Ed.*, 2009, **48**, 9121–9123.
5 L. Huang, Q. Liao, Q. Shi, H. Fu, J. Ma and J. Yao, *J. Mater. Chem.*, 2010, **20**, 159–166.
6 X. Zhang, X. Zhang, K. Zou, C. S. Lee and S. T. Lee, *J. Am. Chem. Soc.*, 2007, **129**, 3527–3532.
7 A. Masuhara, Z. Tan, H. Kasai, H. Nakanishi and H. Oikawa, *Jpn. J. Appl. Phys.*, 2009, **48**, 050206.
8 T. Herricks, J. Chen and Y. Xia, *Nano Lett.*, 2004, **4**, 2367–2371.
9 X. Huang, Z. Zhao, J. Fan, Y. Tan and N. Zheng, *J. Am. Chem. Soc.*, 2011, **133**, 4718–4721.
10 M. Jin, H. Zhang, Z. Xie and Y. Xia, *Angew. Chem., Int. Ed.*, 2011, **50**, 7850–7854.
11 H. Khurshid, W. Li, S. Chandra, M. H. Phan, G. C. Hadjipanayis, P. Mukherjee and H. Srikanth, *Nanoscale*, 2013, **5**, 7942–7952.
12 B. Lim and Y. Xia, *Angew. Chem., Int. Ed.*, 2011, **50**, 76–85.
13 A. R. Poerwoprajitno, L. Gloag, S. Cheong, J. J. Gooding and R. D. Tilley, *Nanoscale*, 2019, **11**, 18995–19011.
14 H. X. Ji, J. S. Hu, Q. X. Tang, W. G. Song, C. R. Wang, W. P. Hu, L. J. Wan and S. T. Lee, *J. Phys. Chem. C*, 2007, **111**, 10498–10502.
15 S. Mostafa Nowee, A. Abbas and J. A. Romagnoli, *Chem. Eng. Sci.*, 2008, **63**, 5457–5467.
16 W. Li, C. Zhao, B. Zou, X. Zhang, J. Yu, X. Zhang and J. Jie, *CrystEngComm*, 2012, **14**, 8124–8127.
17 P. MacFhionnghaile, V. Svoboda, J. McGinty, A. Nordon and J. Sefcik, *Cryst. Growth Des.*, 2017, **17**, 2611–2621.
18 S. Zheng, N. T. Cuong, S. Okada, T. Xu, W. Shen, X. Lu and K. Tsukagoshi, *Chem. Mater.*, 2018, **30**, 7146–7153.
19 C. Park, E. Yoon, M. Kawano, T. Joo and H. C. Choi, *Angew. Chem., Int. Ed.*, 2010, **49**, 9670–9675.
20 L. K. Shrestha, Y. Yamauchi, J. P. Hill, K. Miyazawa and K. Ariga, *J. Am. Chem. Soc.*, 2013, **135**, 586–589.
21 J. Kim, C. Park and H. C. Choi, *Chem. Mater.*, 2015, **27**, 2408–2413.
22 S. Zheng and X. Lu, *RSC Adv.*, 2015, **5**, 38202–38208.
23 N. Chen, Y. Hu, T. Xu and X. Lu, *ACS Appl. Electron. Mater.*, 2020, **2**, 2010–2016.
24 Y. Xu, X. Chen, F. Liu, X. Chen, J. Guo and S. Yang, *Mater. Horiz.*, 2014, **1**, 411.
25 P. Bairi, K. Minami, J. P. Hill, K. Ariga and L. K. Shrestha, *ACS Nano*, 2017, **11**, 7790–7796.
26 J. Wu, X. Zhu, Y. Guan, Y. Wang, F. Jin, R. Guan, F. Liu, M. Chen, Y. Tian and S. Yang, *Angew. Chem., Int. Ed.*, 2019, **58**, 11350–11354.
27 Y. Wang, J. He, C. Liu, W. H. Chong and H. Chen, *Angew. Chem., Int. Ed.*, 2015, **54**, 2022–2051.
28 A. K. Cheetham, G. Kieslich and H. H.-M. Yeung, *Acc. Chem. Res.*, 2018, **51**, 659–667.
29 S. R. Marsden, L. Mestrom, D. G. G. McMillan and U. Hanefeld, *ChemCatChem*, 2020, **12**, 426–437.
30 A. Einstein, *Ann. Phys.*, 1905, **322**, 549–560.
31 Y. Park, K. Song and H. C. Choi, *CrystEngComm*, 2021, **23**, 777–782.
32 Z. Lou, B. Huang, X. Qin, X. Zhang, H. Cheng, Y. Liu, S. Wang, J. Wang and Y. Dai, *Chem. Commun.*, 2012, **48**, 3488.
33 Y. Yin and A. P. Alivisatos, *Nature*, 2005, **437**, 664–670.
34 H. Dong, C. Zhang, F. Shu, C. Zou, Y. Yan, J. Yao and Y. S. Zhao, *Adv. Mater.*, 2021, **33**, 2100484.
35 E. H. Archibald and W. Ure, *J. Chem. Soc., Trans.*, 1924, **125**, 726–731.